Hindawi
Advances in Materials Science and Engineering
Volume 2020, Article ID 6505301, 16 pages
https://doi.org/10.1155/2020/6505301

Research Article

Effect of Surface Site Defects on Photocatalytic Properties of $BiVO_4/TiO_2$ Heterojunction for Enhanced Methylene Blue Degradation

Sahar Mansour, Rym Akkari, Semy Ben Chaabene, and Mongia Saïd Zina

Université de Tunis El Manar, Faculté des Sciences de Tunis, LR08ES01 Laboratoire de Chimie des Matériaux et Catalyse, 2092, Tunis, Tunisia

Correspondence should be addressed to Sahar Mansour; mansoursahar593@gmail.com

Received 30 July 2020; Revised 22 October 2020; Accepted 5 December 2020; Published 15 December 2020

Academic Editor: Pramod Koshy

Combining a super photoresponsive $BiVO_4$ catalyst to the large band gap TiO_2 material seems to be a great interest in order to improve the visible-light-driven photodegradation of hazardous pollutants. $BiVO_4/TiO_2$ heterojunction composites have been synthesized via a simple one-pot hydrothermal route. Herein, we carefully highlighted the effect of $BiVO_4$ content on the physicochemical and photocatalytic properties of solids towards the decomposition of methylene blue (MB) under solar light irradiation. The main results revealed that the formation of the heterostructures catalyst by incorporating $BiVO_4$ into TiO_2 stabilizes the anatase phase of TiO_2 by inhibiting its crystal growth and improves significantly the light absorbance of titanium dioxide. The results showed that the best photocatalytic performance is assigned to the catalyst with 2 wt% $BiVO_4$ loading which is higher than both pure $BiVO_4$ and TiO_2. This improvement of photocatalytic activity is related to the synergetic effect between both materials. Furthermore, the constructed junction leads to an increase in the concentration of oxygen defects on the semiconductor surface which could create an acceptor energy level into the valence band of TiO_2. Four cyclic runs for the photocatalytic degradation of MB on $BiVO_4/TiO_2$ composite revealed its stability and sustainable reusability.

1. Introduction

Dye effluents pose serious ecotoxic problems. Methylene blue (MB) is one of the organic dyes which are present in the textile effluents [1]. In addition to its toxicity, the presence of MB in aquatic systems could be the origin of serious damages to human health [2].

In this regard, enormous efforts have been devoted in order to get rid of these recalcitrant compounds. Photocatalytic degradation using heterojunction semiconductors is one of the most promising technologies for preventing global environmental pollution [3, 4]. Several semiconductors have been analyzed in heterogeneous photocatalysis such as Fe_2O_3, ZnO, CdS, and ZnS [5–9]. Among the wide range of semiconductors, titanium dioxide (TiO_2) is well recognized as the most effective material in photocatalytic applications due to its strong catalytic properties [10, 11]. Nevertheless, because of its wide band gap, TiO_2 presents a limited absorption in the visible light range together with a rapid recombination of photoinduced charge carriers which restricts its practical applications [12, 13].

Therefore, one of the greatest challenges for improving the photoactivity of TiO_2 is to increase the carrier lifetime and enhance the absorption in the visible light range. This is feasible by modifying the titanium dioxide surface by doping [14], self-doping [15], or coupling with other oxides [16, 17]. Among the proposed approaches, the construction of heterojunction photocatalysts is a potential pathway because coupling TiO_2 with a narrow band gap semiconductor participates in a more powerful separation of the photogenerated electron-hole pairs [18].

As reported in the previous literature, bismuth vanadate ($BiVO_4$) has attracted substantial attention of several researchers owing to many advantages such as nontoxicity,

photochromic effect, resistance to corrosion, and high photostability [19, 20].

It was mentioned that $BiVO_4$ exists mainly in three crystalline polymorphs: tetragonal scheelite (t-$BiVO_4$), monoclinic scheelite (m-$BiVO_4$), and tetragonal zircon structures (tz-$BiVO_4$) [21]. In a comparative study between the different crystalline phases [22], it was pointed out that monoclinic $BiVO_4$ (m-$BiVO_4$) shows the highest photocatalytic activity for the degradation of organic pollutants from wastewater [23].

In this respect, combining both powerful photooxidation capacity of TiO_2 and strong visible light absorption provided by $BiVO_4$ can potentially be achieved by forming heterostructured photocatalysts based on m-$BiVO_4$/TiO_2 for greater photocatalytic performances.

Song et al. [24] have shown that the construction of $BiVO_4$/P25 heterostructure promotes the creation of oxygen defects on the photocatalyst surface. These defects allow trapping the photogenerated electrons and enhance the charge separation, which ameliorates the photoactivity of catalysts.

Monfort et al. [25] synthesized $BiVO_4$/TiO_2 nanocatalysts via a simple sol-gel method, and they evaluated their activity in water splitting. They recorded the highest H_2 production for the $BiVO_4$/TiO_2 framework due to the intimated contact between $BiVO_4$ and TiO_2.

Zhu et al. [26] reported the elaboration of $BiVO_4$/TiO_2 heterojunction containing Ti^{3+} species as defect centers by a two-step hydrothermal route. The elaborated nanocomposites exhibit a photoactivity 7 times higher than pure $BiVO_4$ and pure TiO_2 towards the phenol degradation. This could be due to the presence of Ti^{3+} which establishes an intermediate energy level, enhancing the electron transfer property.

The $BiVO_4$/TiO_2 nanocomposites synthesized by the simple coupling method (sol-gel and hydrothermal methods) exhibited high photocatalytic activity for the oxidation of RhB with a yield that reached 80%. The results have provided further evidence that the $BiVO_4$ loading enhances considerably the decomposition of RhB dye, and this was attributed to the presence of $O^{2\bullet-}$ and $OH^{\bullet}$ active species [27].

A study carried out by Rangel and coworkers [28] proved that the hydrothermal method increases the defect concentration, creating intermediate levels in the band gap energy which in turn improves the photoresponse of catalysts in the visible light range.

To the best of our knowledge, no studies on the photodegradation of methylene blue using $BiVO_4$/TiO_2 heterojunction prepared via a one-step hydrothermal elaboration have been reported; hence, the originality of this investigation.

In the current study, $BiVO_4$/TiO_2 heterojunction nanocomposites were synthesized using a one-pot hydrothermal method. The introduction of the $BiVO_4$ effect on the structural, textural, optical, and photocatalytic activities of $BiVO_4$/TiO_2 nanocomposites was studied in detail. The photocatalytic performances of the coupled catalysts were investigated for the degradation of MB under solar light irradiation, and a possible photocatalytic mechanism was proposed. Furthermore, a stability and reusability study was carried out in order to ensure its sustainable use as a promising photocatalyst in the wastewater treatment field.

2. Materials and Methods

2.1. Materials. Titanium isopropoxide ($Ti(OiPr)_4$, 97%) was purchased from Sigma-Aldrich and used as a titanium source. Nitric acid (HNO_3, solution 65% w/w) provided by Scharlau was employed as a peptizing agent. Bismuth nitrate ($Bi(NO_3)_3$, 99%) and ammonium metavanadate (NH_4VO_3, 99%) were obtained from Acros and used as the bismuth vanadate source. Ethanol (C_2H_5OH, 99.5%) was supplied from Sigma and used for washing solids. Sodium hydroxide (NaOH, 98%) was purchased from Aldrich and used to dissolve NH_4VO_3. Methylene blue (Sigma-Aldrich, ≥82%) was utilized as a model molecule in the photocatalytic reaction. All chemicals were analytical grade without further treatment.

2.2. Elaboration of $BiVO_4$/TiO_2 Photocatalysts. $BiVO_4$ was introduced into the TiO_2 material by a hydrothermal method in order to obtain 2, 5, and 10 wt% $BiVO_4$ loading in the final $BiVO_4$/TiO_2 composite.

2.2.1. $BiVO_4$/TiO_2 Composite Synthesis by Hydrothermal Route. The $BiVO_4$/TiO_2 catalyst was prepared using the following protocol (Figure 1): 0.59 g of $BiNO_3$ was first dissolved in an aqueous solution of nitric acid (4 mol·L^{-1}) to form solution *A*. Then, solution *B* was obtained by dissolving 0.18 g of NH_4VO_3 into NaOH aqueous solution (2 mol·L^{-1}). Afterward, the solution *A* was poured drop by drop in solution *B* until the formation of an intense yellow suspension. The obtained $BiVO_4$ suspension was subsequently added dropwise to a TiO_2 sol which was prepared as follows: a well-defined volume of titanium isopropoxide necessary to fix its concentration to 1 mol·L^{-1} was added to an aqueous solution of nitric acid (4 mol·L^{-1}). The mixture was stirred for 24 h at 40°C. The pH of the solution was adjusted to 7 by dripping the NaOH solution (4 mol·L^{-1}). The obtained mixture was then transferred to a Teflon stainless steel autoclave and heated at 180°C for 24 h. After recovering from the autoclave, the as-obtained materials were washed several times with distilled water and ethanol and left drying at 100°C for 7 h.

All composites were heat treated under oxygen flow at 500°C for 3 h.

2.3. Catalysts Characterization. The structure and the particle sizes of as-synthesized $BiVO_4$/TiO_2 composites were examined by powder X-ray diffraction (X'Pert Pro (PW3040/60) diffractometer equipped with a Cu-Kα radiation source ($\lambda = 0.154$ nm) in the scanning range of 20–80°). Raman spectra measurements were carried out on a Lab-RAM (Horiba scientific) using a green line of 563 nm Ar-laser as the excitation source. The morphologies of the

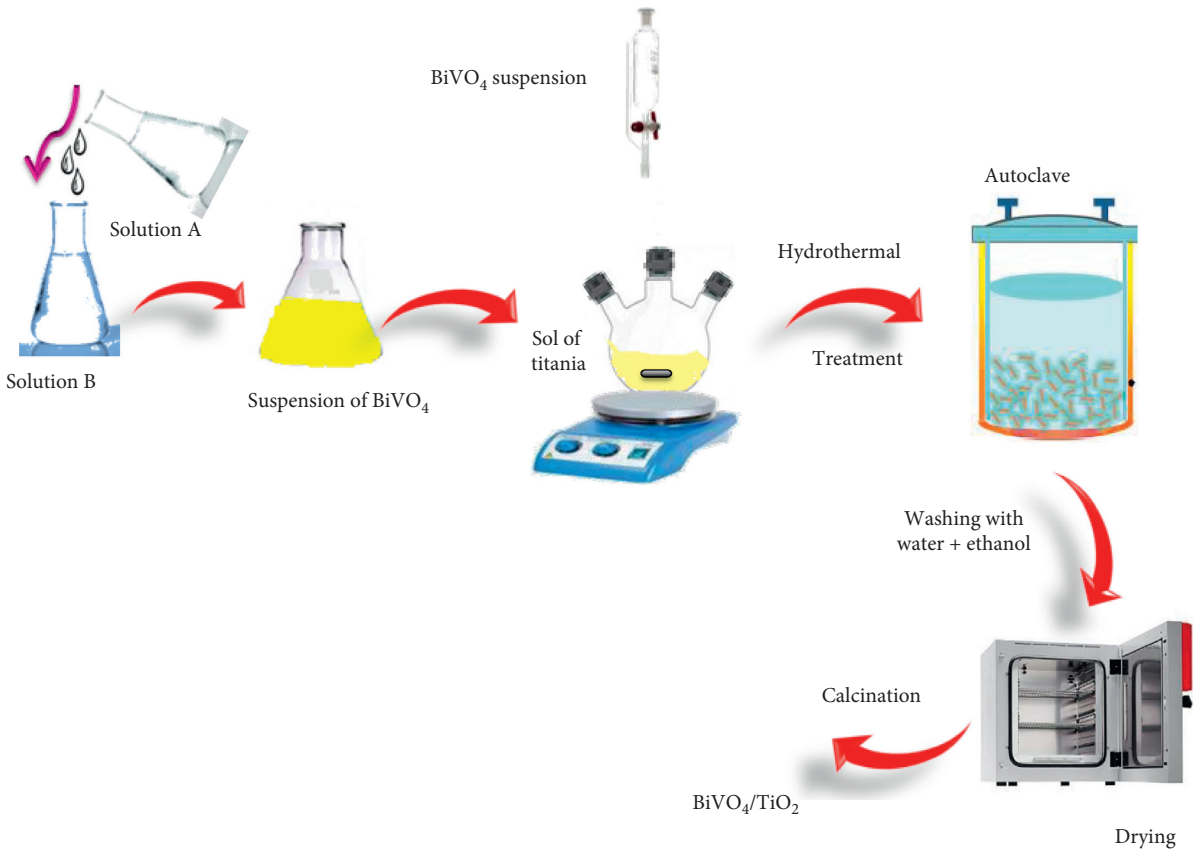

Figure 1: Experimental protocol of $BiVO_4/TiO_2$ synthesis.

$BiVO_4/TiO_2$ samples were studied by scanning electron microscopy imaging with a SEM type JEOL JSM-6460LV apparatus. High-resolution transmission electron microscopy (HRTEM) was employed to observe the heterojunction formation of $BiVO_4/TiO_2$ nanocomposite through HRTEM JEOL JEM-ARM 200F.

The Brunauer–Emmett–Teller (BET) surface area and porosity were measured by N_2 adsorption-desorption at 77 K on an automatic Micrometritics ASAP 2020 analyzer. X-ray photoelectron spectroscopy (XPS) investigations of the catalysts were also recorded with a VG Escalab 200R spectrometer equipped with the monochromatic Mg Kα radiation ($h\nu = 1253.6$ eV) X-ray source. UV-vis-NIR Varian Cary 5000 spectrometer was used in order to analyze the UV-vis spectra of the photocatalysts in the wavelength rage of 200–700 nm. The photoluminescence spectra were recorded via a Perkin Elmer Lambda S55 (LS55) spectrophotometer equipped with a xenon lamp excitation wavelength of 300 nm.

2.4. Photocatalytic Activity Test. The photocatalytic performances of the as-prepared catalysts were examined in the degradation of methylene blue (MB) in aqueous solution and under solar light irradiation. This reaction was then performed at room temperature. Typically, 50 mg photocatalyst was suspended into 100 mL of MB solution (10 mg·L^{-1}) in a Pyrex glass vessel. In order to reach the adsorption-desorption equilibrium between MB and photocatalyst surface, the suspensions were magnetically stirred in darkness for 45 min prior to irradiation. Subsequently, the mixture was irradiated with solar light for 60 min. The luminous flux emitted by solar radiation was measured by a radiometer equipped with a detector, and it is close to 1,743 mWcm^{-2}. The photodegradation process was followed using a Shimadzu UV-3600 spectrophotometer at a wavelength $\lambda_{max} = 665$ nm which is the maximum absorption of MB. The photodegradation rate was calculated according to Beer–Lambert's law [29]:

$$\text{Degradation efficiency}\,(\%) = \frac{A_0 - A_t}{A_0} \times 100, \quad (1)$$

where A_0 is the initial absorbance of MB, and A_t is the absorbance after irradiation at time t.

3. Results and Discussion

3.1. Structural and Morphological Properties

3.1.1. XRD Analysis. Figure 2 illustrates the X-ray diffractograms of the $BiVO_4/TiO_2$ composites prepared using hydrothermal route and calcined at 500°C.

The XRD pattern of bare $BiVO_4$ was in good agreement with the monoclinic scheelite $BiVO_4$ phase according to JCPDS No. 14–0688. For pure TiO_2, the diffraction peaks attributed to the anatase phase at 25.3°, 37.9°, 48.1°, 54.0°,

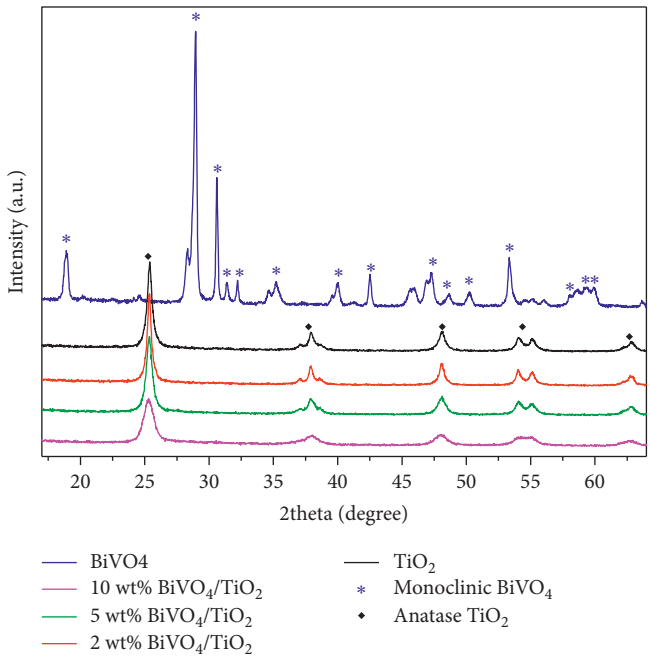

FIGURE 2: XRD patterns of pure TiO_2, pure BVO_4, and $BiVO_4/TiO_2$ nanocomposites with different $BiVO_4$ contents.

55.2°, and 62.8° could be perfectly assigned to the (101), (004), (200), (105), (211), and (204) crystal diffraction planes of anatase TiO_2 according to the database of JCPDS card No. 21–1272. The diffraction peaks of the as-prepared $BiVO_4/TiO_2$ solids with different contents exhibit only the characteristic peaks of the TiO_2 anatase phase. For all the samples, no characteristic peaks of $BiVO_4$ or any impurity were observed in their XRD patterns which indicate that $BiVO_4$ is well dispersed onto the TiO_2 surface. These results showed the presence of only anatase TiO_2 which corroborates well that the combination of these two semiconductors preserves the crystalline structure of TiO_2. It is clear that increasing the $BiVO_4$ leads to a reduction of the diffraction peaks intensities of samples suggesting the possible decrease of TiO_2 crystallinity. To gain further understanding on this finding, Zhang et al. [30] reported that the lattice distortion of the substrate and the presence of site defects on the surface of the matrix are the main causes of the crystallinity lessening. These outcomes matched well with the results of the lattice parameters of samples which recorded a slight variation of the *c*-axis lattice parameter, as well as the unit cell volume, compared to pristine TiO_2. It is possible to infer that the introduction of $BiVO_4$ by hydrothermal treatment could distort the TiO_2 network. These observations are in good agreement with observations made by Yang et al. [31] who highlighted that interstitial doping leads to an extension of the network structure of titanium dioxide along the *c*-axis.

Table 1 shows the average crystallite size of the as-synthesized composites which were calculated by applying Scherrer's formula [32] using the line width of the (101) diffraction peak of TiO_2. Results show that the average crystallite size of the prepared materials is between the sizes of pure TiO_2 and $BiVO_4$. According to this table, it can be seen that the introduction of $BiVO_4$ has significantly reduced the crystallite size compared to pristine TiO_2. These findings are in good agreement with observations made by Song et al. [24]. In fact, the authors proved that an appropriate amount of $BiVO_4$ could inhibit the crystallite growth of TiO_2. This is probably due to the fact that the crystalline growth of $BiVO_4$ which starts into the surface of TiO_2 is highly affected by the establishment of chemical interactions between the two materials. In fact, the Bi^{3+} and V^{5+} species remaining in the solution could participate in the germination process and crystal growth. Thereby, a strong interaction between Bi^{3+}, V^{5+} species, and titanium alkoxide could explain this observation. In this case, the TiO_2 crystal growth around $BiVO_4$ nanoparticles could be probably influenced by the establishment of chemical bonds between the two species which lead probably to the distortion of the titanium dioxide lattice.

3.1.2. Raman Spectroscopy. The determination of the vibrational transitions, the bounding states in the crystal lattice, and the local distortion of the solid can be studied with Raman spectroscopy which is considered herein as a performing technique to better discern the effect of $BiVO_4$ on the local structure of TiO_2. The Raman spectra of composites with the scope of 100–1000 cm^{-1} are reported in Figure 3. Raman spectrum analysis of pristine $BiVO_4$ (Figure 3(a)) shows the presence of six typical vibrational bands at 821, 706.3, 364.2, 331.3, 209.6, and 123.7 cm^{-1} which are characteristic of monoclinic scheelite phase of $BiVO_4$ and confirming the XRD results. The intense band at 821 cm^{-1} is assigned to the symmetric *V-O* stretching mode in *V* units with a small shoulder at 706.3 cm^{-1} assigned to antisymmetric *V-O* vibrations. The bands appearing at 331.3 and 364.2 cm^{-1} are attributed to the bending vibration of *V-O* bonds. Likewise, two peaks located at 209.6 cm^{-1} and 123.7 cm^{-1} are assigned to the rotational and translational vibrations, respectively [33]. Raman spectrum of bare TiO_2 and mixed oxides with different $BiVO_4$ contents show only the appearance of characteristic anatase Raman vibrations at 146.8, 197.7, 399.2, 515.6, and 641 cm^{-1} which correspond, respectively, to the active lattice vibrations modes E_{1g}, E_{2g}, B_{1g}, A_{1g}/B_{1g}, and E_g [34]. No peaks corresponding to the scheelite monoclinic $BiVO_4$ phase were observed. Thereby, the addition of $BiVO_4$ leads to a significant reduction of the peak intensity related to the E_g active mode of anatase at 146.8 cm^{-1} for mixed oxides and especially at low content (2 wt% $BiVO_4/TiO_2$) in comparison with pure TiO_2 which exhibits an intense peak. This is probably due to the presence of site defects in the surface of solids. Furthermore, the observed spectra shown in Figure 3(b) allows discerning that bismuth vanadate causes a slight shift (1.5 cm^{-1}) of the main band (146.8 cm^{-1}) to higher wavenumbers suggesting the increase of oxygen vacancies [35]. The highlighted conclusion from this observation is the effect of $BiVO_4$ in the generation of oxygen site defects which originates from the deformation of the TiO_2 lattice after its modification following $BiVO_4$ introduction.

Table 1: Structural parameters of pure TiO_2, pure $BiVO_4$, and $BiVO_4/TiO_2$ nanocomposites determined from XRD data.

Catalysts	XRD crystallite size (nm)	a (Å)	b (Å)	c (Å)	Unit cell volume (Å^3)
TiO_2	54	3.78	3.78	9.51	135.88
2 wt% $BiVO_4/TiO_2$	18	3.78	3.78	9.50	135.93
5 wt% $BiVO_4/TiO_2$	22	3.78	3.78	9.51	136.27
10 wt% $BiVO_4/TiO_2$	31	3.78	3.78	9.53	136.93
$BiVO_4$	45	5.17	5.10	11.67	308.55

3.1.3. SEM Analysis. The scanning electron microscopy images of pure $BiVO_4$, pure TiO_2, and 2 wt% $BiVO_4/TiO_2$ samples are depicted in Figure 4. An enlarged SEM micrograph of pristine $BiVO_4$ (Figures 4(a) and 4(b)) shows that the latter exhibits a pinwheel-like shape. Figure 4(c) indicates that the particle distribution of the sample TiO_2 is aleatory and the grains are large with heterogeneous size since random distribution causes agglomeration of grains [36]. The 2 wt% $BiVO_4/TiO_2$ nanocomposite (Figure 4(d)) has a morphology similar to pure TiO_2 but with smaller particle size. It is clearly seen that the $BiVO_4$ reduced the size of the titanium dioxide nanoparticles which fits well with the XRD results.

3.1.4. TEM Analysis. The nanomorphology of Pt-BV/T(X) photocatalysts was analyzed by TEM and HRTEM (Figure 5). TEM micrographs of 2 wt% $BiVO_4/TiO_2$ nanocomposite (Figure 5(a)) exhibited a heterogeneous structure of nanoparticles which is composed of a mixture of nanospheres and small nanorods with an average size of approximately 14.62 nm. As shown by HRTEM (Figure 5(b)), the measured spacing of nanoparticles is 0.35 nm which corresponds to the (101) crystallographic plane of TiO_2, while the interplanar distance of 0.308 nm was indexed to the (121) planes of $BiVO_4$ [37, 38]. HRTEM image clearly showed the formation of $BiVO_4/TiO_2$ heterojunction with great interaction between $BiVO_4$ and TiO_2.

3.2. Textural and Surface Properties

3.2.1. N_2 Adsorption-Desorption Analysis. A series of nitrogen adsorption-desorption isotherms at 77 K were performed as shown in Figure 6. According to the IUPAC classification [39], the as-prepared composites exhibited a type IV (a) isotherm characteristic of the mesoporous materials with several types of hysteresis loops. In fact, an H_2 (b) hysteresis loop was attributed to the bare TiO_2. 2 wt% and 5 wt% $BiVO_4/TiO_2$ and the pure $BiVO_4$ samples display an H_3 hysteresis loop characteristic of nonrigid aggregates of plate particles with slit-shaped pores. For the 10 wt% $BiVO_4/TiO_2$ sample, an overlapping of both H_3 and H_2 (b) hysteresis loops was observed. The pore size distribution curves of materials (Figure 7) show monomodal patterns. It can be seen that increasing the $BiVO_4$ loading shifts the pore size distribution to lower pore diameter values except for 5 wt% loading. This could be probably due to the reduction of the intraparticle pore size [40].

The relative pressure range indicates that earlier is the onset of the loops, smaller is the diameter of the mesopores. Table 2 lists the relative pressures P/P° of the hysteresis loops onset of the as-synthesized materials. Outcomes revealed that the addition of $BiVO_4$ increases the relative pressure P/P° of the onset of the hysteresis loop for the catalysts except for 10 wt% loading. This fits well with the BJH pore size distribution which confirms that pure TiO_2 having the smallest P/P° value (0.73) exhibits the smallest pore diameter (169 Å). The relative pressure value of 10 wt% $BiVO_4/TiO_2$ (0.75) agrees well with the result of porous diameter (188). However, it does not follow the linear trend with the percentage of $BiVO_4$. This could probably be due to the start of a change in the hysteresis loop from H_{2b} to H_3. Thereby, it is obvious to highlight the important effect of $BiVO_4$ on the texture and its importance in the control of the mesopores sizes and the particles morphologies. Compared to $BiVO_4$, the $BiVO_4/TiO_2$ composites have higher specific surface areas and larger pore volume but smaller pore size, and compared to the pure TiO_2, the incorporation of $BiVO_4$ seems to improve the textural properties of the materials. These results are in good agreement with the specific surface area (Table 2). The obtained results showed that the surface area of samples exhibits improvement after the introduction of $BiVO_4$ ranging from 67 m^2g^{-1} for the $BiVO_4$ free TiO_2 to 94 m^2g^{-1} for 10 wt% $BiVO_4/TiO_2$.

3.2.2. X-Ray Photoelectron Spectroscopy. In order to ascertain the formation of $BiVO_4$ on the surface of TiO_2 and investigate the valence state of bismuth and vanadium, an XPS test was performed on the 2 wt% $BiVO_4/TiO_2$ catalyst. Table 3 shows the existence of Ti, *O*, Bi, and *V* species. The characteristic peaks of Ti^{4+} in the tetragonal structure (Ti $2p_{3/2}$ and Ti $2p_{1/2}$) were centered at 458.6 eV and 464 eV, respectively [41]. The summary of XPS results given in Table 3 revealed the presence of the lattice oxygen corresponding to the peaks at 530.2 eV which is inherent to the Ti-*O*-Ti bonds [42]. Figure 8 displays the XPS survey spectra of the sample which confirms the presence of Bi and *V*. As shown in Figure 8(a), two symmetric photoelectron peaks centered at 517.2 eV and 524.7 eV were assigned to $V2p_{3/2}$ and $V2p_{1/2}$, respectively. The difference in binding energy between $V2p_{3/2}$ and $V2p_{1/2}$ is 7.6 eV proves the +5 oxidation state of vanadium. The split binding energy peaks of $Bi4f_{7/2}$ and $Bi4f_{5/2}$ (Figure 8(b)) were centered, respectively, at 159.2 eV and 164.4 eV. The distance between these two peaks is found to be 5.2 eV which is specific to Bi^{3+} [30] in a typical heterojunction sample [43]. Thereby, the absence of the characteristic peaks of metallic bismuth, bismuth oxide, and bismuth titanate further confirms the presence of the component bismuth in the vanadate state [44]. All of

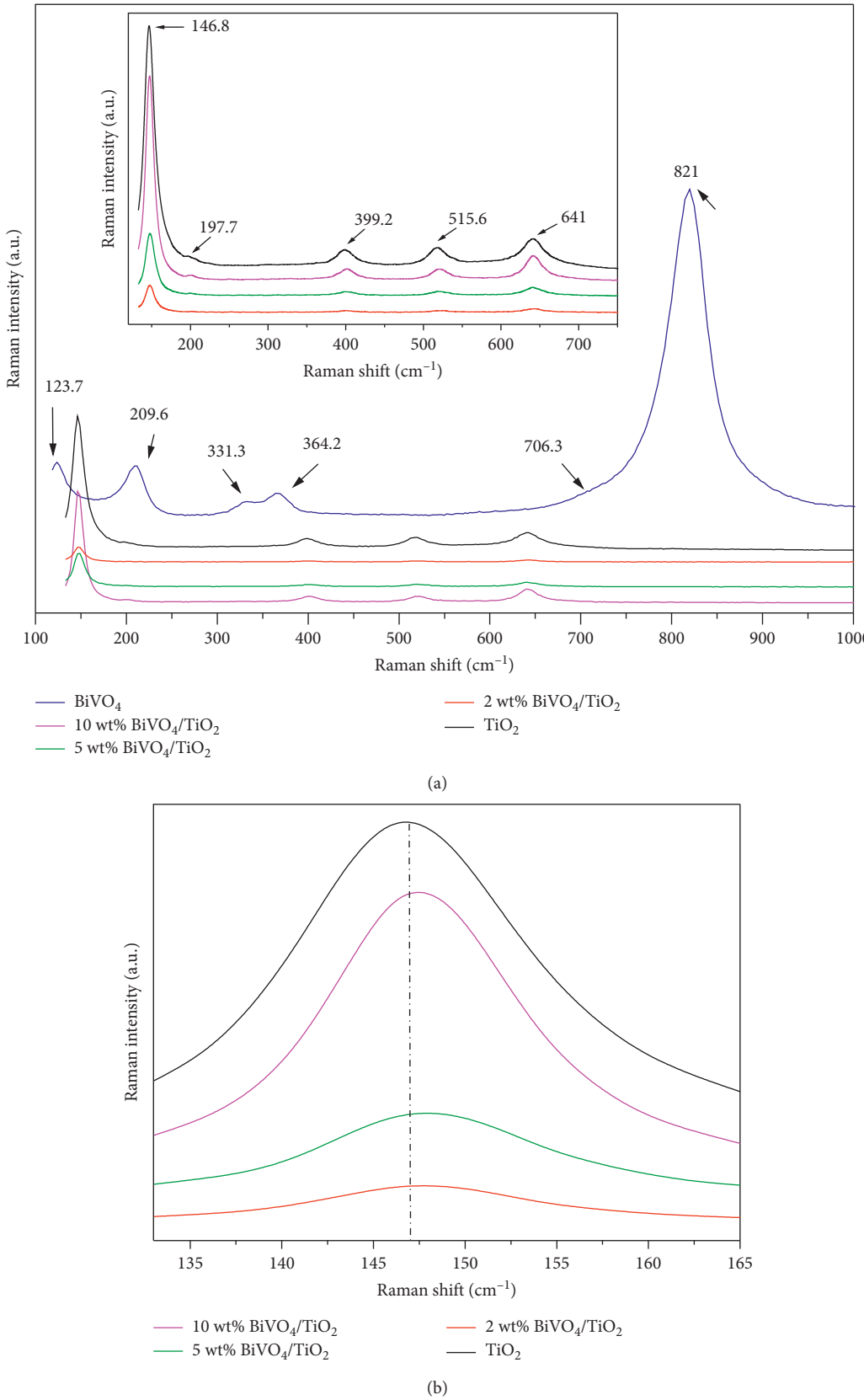

Figure 3: (a) Raman spectra of materials and (b) magnified spectra of the 133–165 cm^{-1} region.

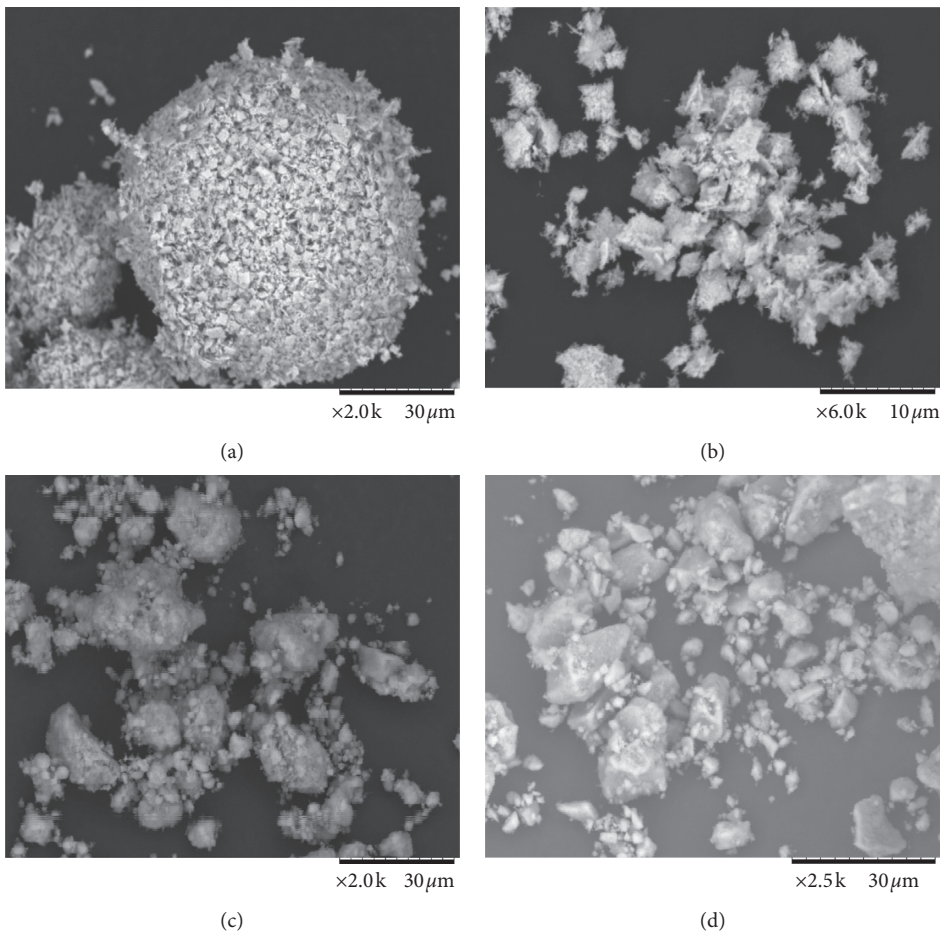

Figure 4: SEM images of the as elaborated samples: (a), (b) $BiVO_4$, (c) TiO_2, and (d) 2 wt% $BiVO_4/TiO_2$.

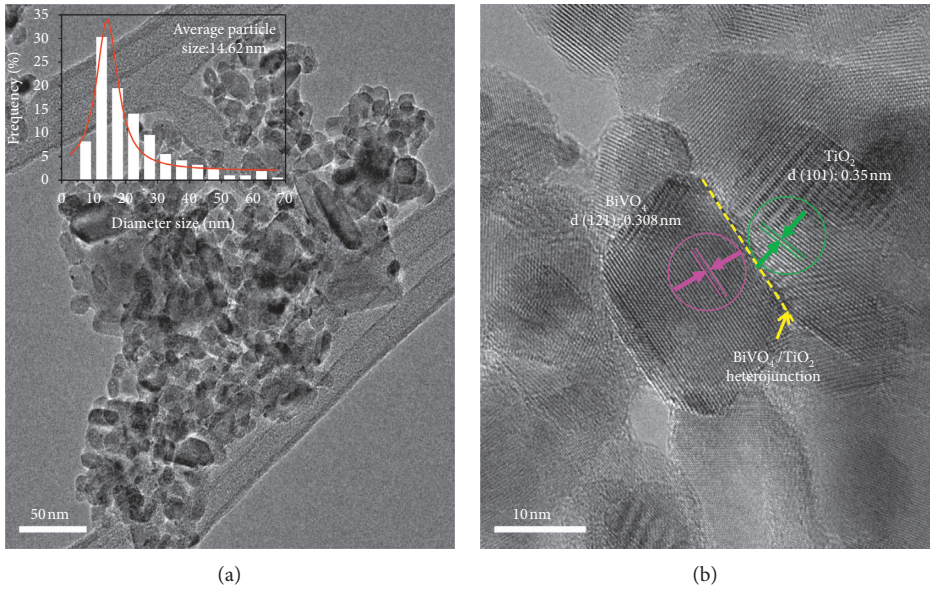

Figure 5: TEM, HRTEM, and average particle size images of 2 wt% $BiVO_4/TiO_2$ nanocomposite.

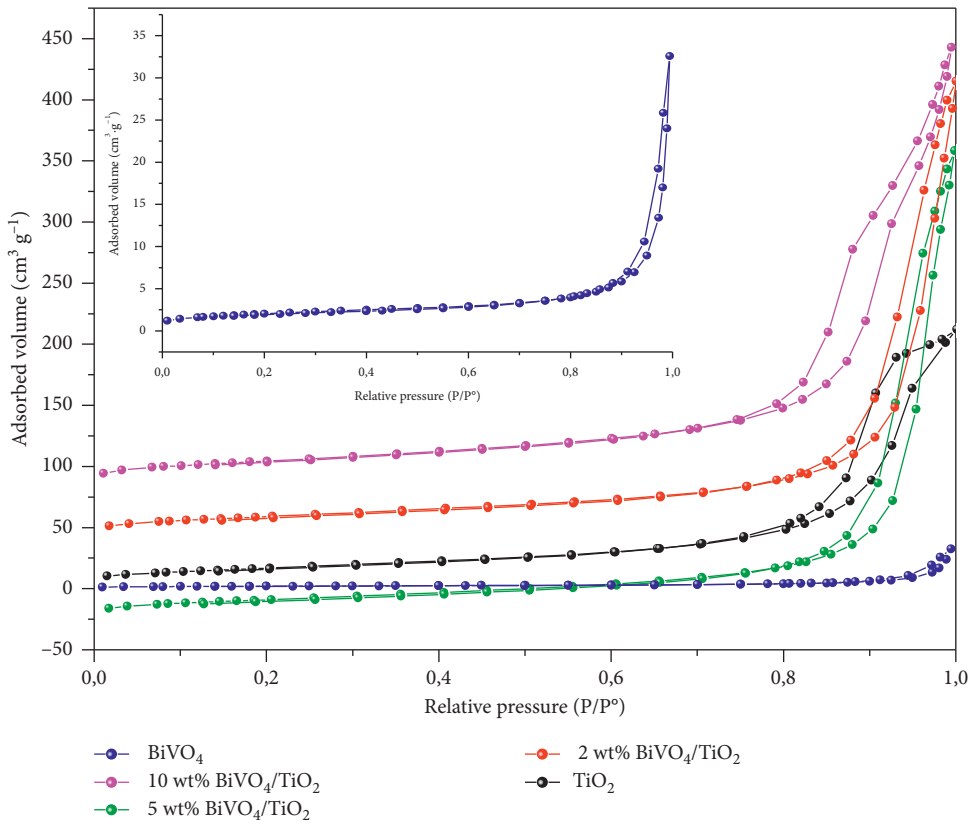

Figure 6: Nitrogen adsorption-desorption isotherm of samples.

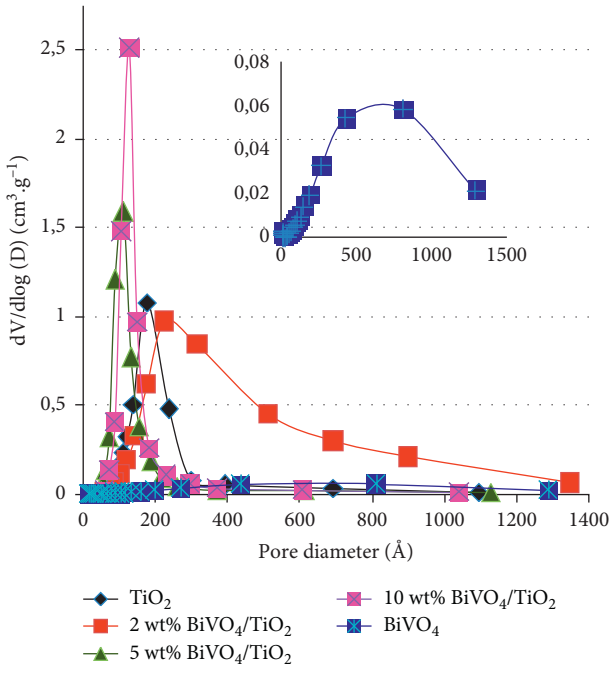

Figure 7: BJH pore size distributions of samples.

these outcomes are testified in favor of the formation of $BiVO_4$. Thereafter, a heterojunction between this latter and TiO_2 is probably created.

3.3. Optical Properties

3.3.1. UV-Vis Diffuse Reflectance Spectroscopy. In order to understand the evolution of the optical properties of $BiVO_4$/TiO_2 nanocomposites compared to pure TiO_2, a series of UV-visible measurements were performed in the wavelength range 250–650 nm as shown in Figure 9. As can be seen, pure TiO_2 showed strong photoresponsiveness in the UV region estimated at 400 nm, whereas that of $BiVO_4$ is around 540 nm which is assigned to the band transition from the Bi 6 s orbital to V 3 d conduction band. It is worth noting that the optical absorption increases very slightly with the $BiVO_4$ incorporation compared to bare titanium dioxide in the visible light range, and it increases with raising the bismuth vanadate content. This finding may be attributed to the coupling effect of both semiconductors. In fact, the construction of a heterojunction between the two materials, pointed out with the XPS technique, increases the defect sites in the TiO_2 lattice creating thus intermediate energy levels between $BiVO_4$ and TiO_2 which is consistent with both our previous XRD and Raman results and the literature [45]. Furthermore, lattice distortion pleads in favor of the creation of more oxygen vacancies which would promote the separation of charge carriers and enhance probably in turn the photocatalytic performances of catalysts.

3.3.2. Photoluminescence Analysis. Photoluminescence (PL) measurements were carried out in order to investigate the migration, transfer, and trapping of the photogenerated

Table 2: Specific surface area (S_{BET}), pore volume, average pore diameter, and onset hysteresis loops (P/P°) of catalysts determined from N_2 chemisorption at 77 K using the BET equation.

Catalysts	S_{BET} (m^2g^{-1})	Pore volume (cm^3g^{-1})	Pore size (Å)	Onset of hysteresis loops (P/P°)
$BiVO_4$	7	0.05	363	0.80
10 wt% $BiVO_4/TiO_2$	94	0.56	188	0.75
5 wt% $BiVO_4/TiO_2$	69	0.59	274	0.79
2 wt% $BiVO_4/TiO_2$	74	0.59	265	0.78
TiO_2	67	0.31	169	0.73

Table 3: Binding energies (eV) of core levels of 2 wt% $BiVO_4/TiO_2$ sample determined from XPS data.

	$Bi4f_{7/2}$	$Bi4f_{5/2}$	$V2p_{3/2}$	$V2p_{1/2}$	O1s	$Ti2p_{3/2}$	$Ti2p_{1/2}$
Binding energy (eV)	159.2	164.4	517.2	524.7	530.2	458.6	464

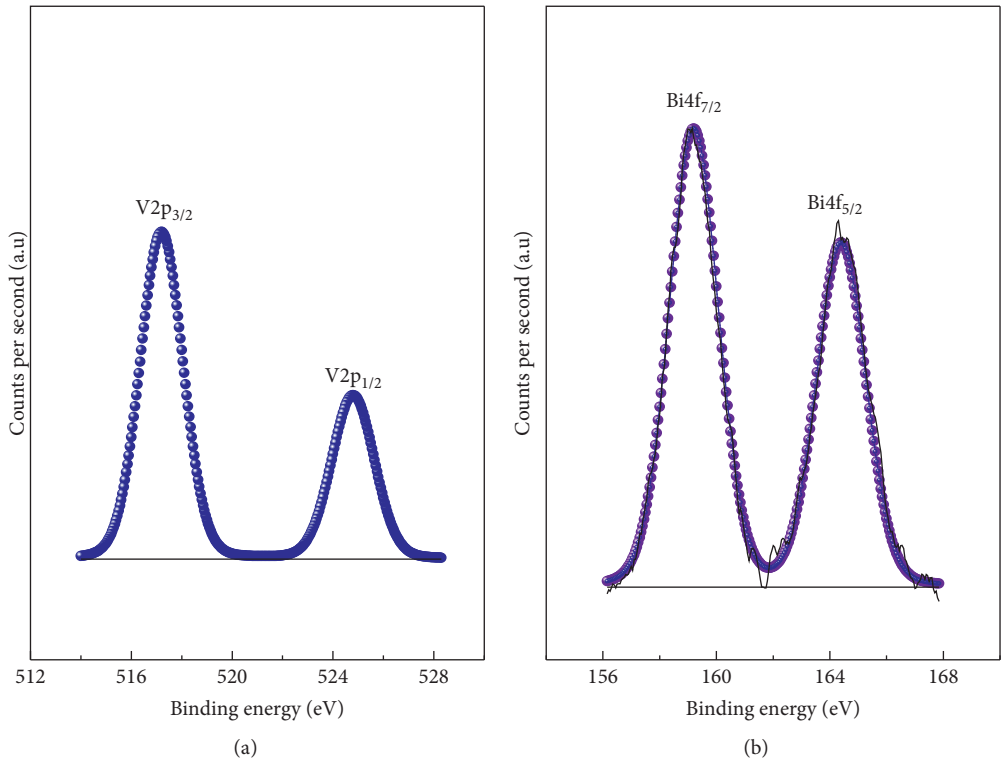

Figure 8: XPS spectra of (a) V2p and (b) Bi_4f of the sample 2 wt% $BiVO_4/TiO_2$.

electron-hole pairs in the titanium dioxide solid. Thus, the photoluminescence is considered as a versatile technique to explore the defect states in the band gap of the semiconductor [46]. Notably, the photoluminescence emission originates from the recombination of photoexcited electron-hole. Therefore, it is well known that a better photocatalytic performance is figured by the lowest recombination rate which is represented by weaker photoluminescence intensity [26]. With the aim of better ascertain the influence of $BiVO_4$ incorporation on the optical properties of TiO_2, the photoluminescence properties of catalysts were examined using an exciting wavelength at 300 nm (Figure 10). The PL spectra of both pure TiO_2 and the $BiVO_4/TiO_2$ nanocomposites were deconvoluted with Gaussian peaks after background subtraction. Careful analysis of deconvoluted PL spectrum of each sample is well fitted by five main emission peaks (Figure 11). The peak centered at 414 nm is related to the recombination of photogenerated electron-hole pairs into the bulk TiO_2 lattice [47]. The peak at 477 nm can be interpreted as the charge transfer from Ti^{3+} to the oxygen anion localized in Ti octahedral [48]. The other peaks at 452 nm and 515 nm are attributed to the recombination of generated electrons with surface oxygen defects [49]. Finally, the emission peak at 558 nm is related to defects and nonstoichiometry in the TiO_2 anatase phase generated by oxygen vacancies [50]. The analysis of the pure $BiVO_4$ spectrum revealed the presence of an emission peak at 500 nm corresponding to the recombination of the electrons in the conduction band of V3d orbital of $BiVO_4$ with the holes formed in the valence band of O2p orbital [26]. Herein,

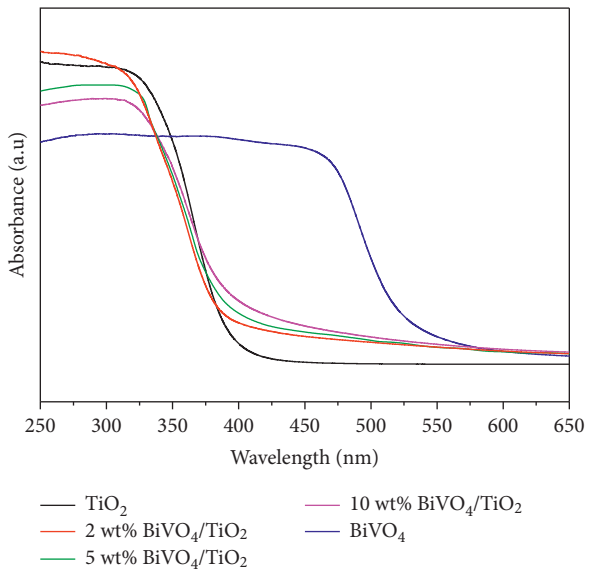

Figure 9: UV-vis absorption spectra of samples.

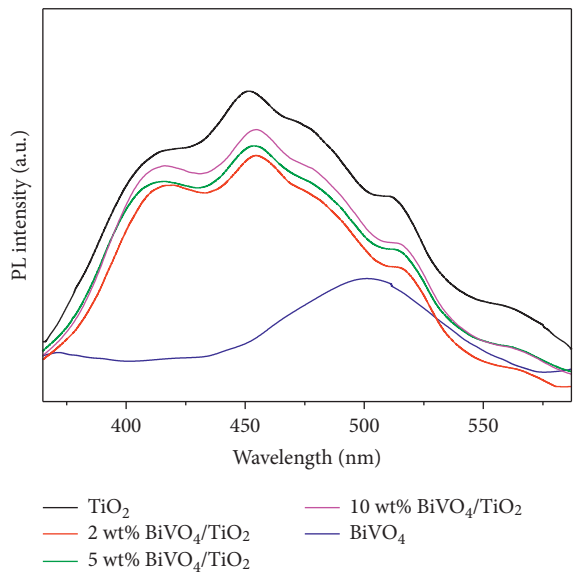

Figure 10: Photoluminescence spectra of photocatalysts.

it is clear that the higher PL intensity of the bare TiO_2 indicates a higher recombination rate. Moreover, results revealed that the PL intensity related to the recombination of electrons with surface oxygen vacancies is a very important factor that determines the photocatalytic performance of the catalyst. Indeed, it is worth noting that these defect sites are capable of trapping photogenerated electrons favoring the reduction of the recombination rate in the $BiVO_4/TiO_2$ composite and enhancing the photocatalytic activity of the as-prepared solids. In this regard, Wetchakun et al. [51] reported that the surface oxygen vacancies could be considered to be the active sites of the $BiVO_4/TiO_2$ material. The PL intensity decreases after the incorporation of $BiVO_4$. This result could be probably due to the formation of a heterojunction which affects the charge separation properties of the photocatalysts. Indeed, we point out that the different positions of the band gap energy between $BiVO_4$ and TiO_2 allow the photogenerated electrons to jump from the $BiVO_4$ valence band to the TiO_2 conduction band [52]. However, the $BiVO_4$ content does not seem to be important in reducing the electron-hole pair recombination rate and only its presence is sufficient to improve the transfer feature of charge carriers.

4. Photocatalytic Activity

The study of the photocatalytic performances of the samples, prepared by the hydrothermal method, was evaluated by measuring the degradation of methylene blue (MB), which was used as a target pollutant, and the investigation of the $BiVO_4$ content's effect on their reactivities. In this respect, photocatalytic activities of samples were estimated by measuring the color removal of MB. As a comparison, the photocatalytic degradation over pure TiO_2 and $BiVO_4$ was performed under the same experimental conditions than the nanocomposites $BiVO_4/TiO_2$. As can be seen from Figure 12, the photocatalytic activity of pristine $BiVO_4$ is very low under solar light irradiation. This finding could be essentially due to its reduced specific surface area ($7\ m^2g^{-1}$) which restricts its adsorption ability towards the decomposition of organic molecules of MB. After coupling $BiVO_4$ and TiO_2, results revealed that MB degradation increases for certain bismuth vanadate amount, and the best photocatalytic conversion is attributed to the 2 wt% $BiVO_4/TiO_2$ composite indicating that 99% of MB was degraded after 60 min. Thereby, the photocatalytic conversion of this material is 2.5 times and 1.25 times higher than that of pure $BiVO_4$ and TiO_2, respectively. Nevertheless, the photocatalytic conversion of 10 wt% $BiVO_4/TiO_2$ is smaller than that of pristine TiO_2 despite its higher surface area. Accordingly, it is worth to note that a high amount of $BiVO_4$ appears to block the active sites [27]. The high conversion which is assigned to the low bismuth vanadate loading could be essentially due to the synergetic effect between $BiVO_4$ and TiO_2 after the heterojunction formation. In fact, Sajjad et al. [53] reported that the creation of a heterojunction increases the photocatalytic performances by its ability to restrict the recombination of the photoinduced electron-hole pairs. Notably, according to Raman spectroscopy analysis, we have shown that the introduction of $BiVO_4$ leads the generation of oxygen surface defects. These oxygen vacancies inducing a TiO_2 lattice distortion can be able to inhibit the crystallite growth which improves the surface area of the catalysts and participate in turn in the separation of charge carriers by trapping the induced photoelectrons. Wang et al. [54] concluded that site defects are the major causes for enhancing the photocatalytic performances of catalysts towards the removal of organic dyes from wastewater. In fact, these defects especially oxygen vacancies, which are considered as a positive electric center, are able to create donor levels in the electronic structure of TiO_2. This pleads in favor of the improvement of the absorption properties of titanium dioxide in the visible light range, on the one hand, and

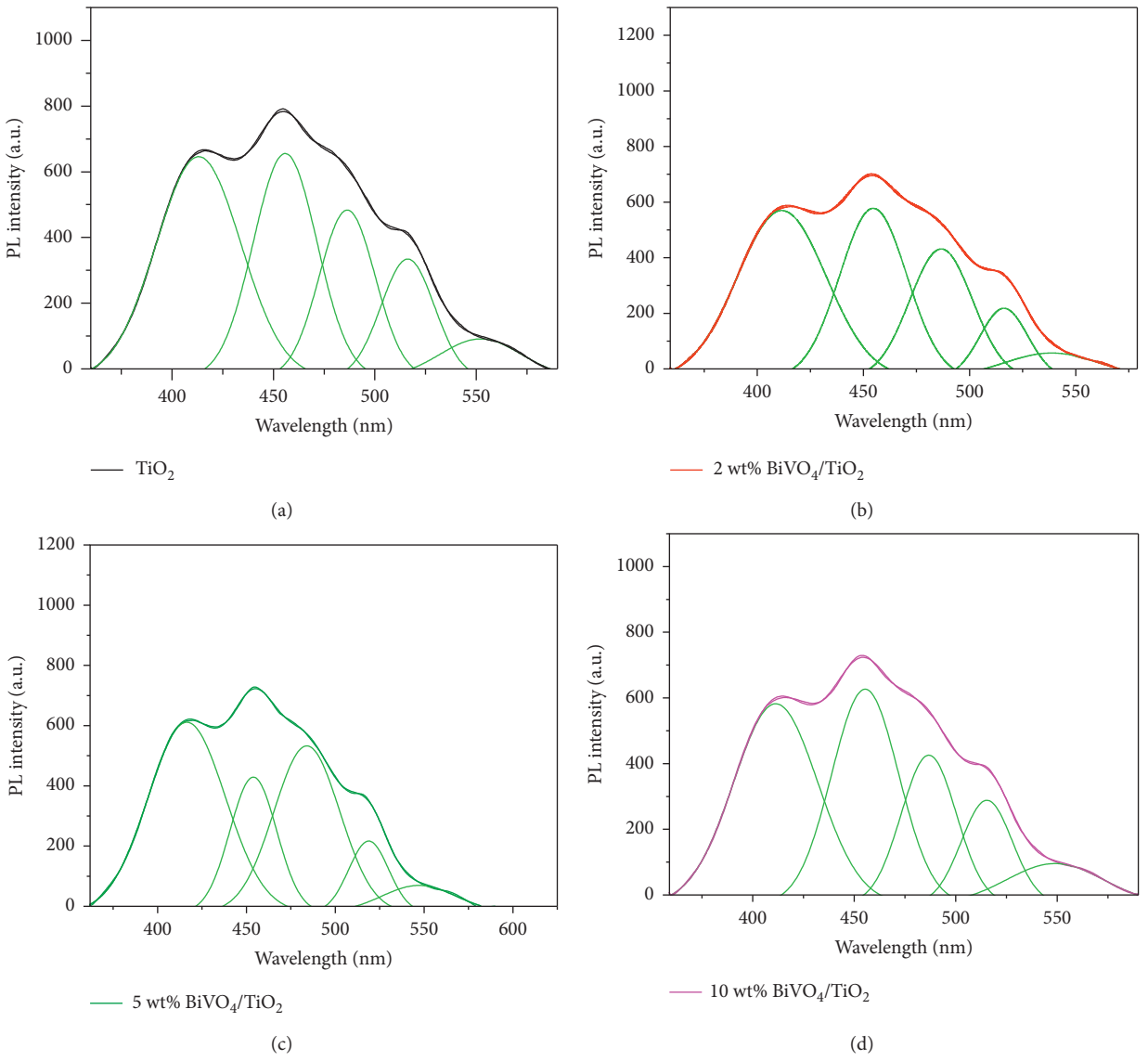

Figure 11: Deconvoluted photoluminescence spectra of (a) TiO_2, (b) 2 wt% $BiVO_4/TiO_2$, (c) 5 wt% $BiVO_4/TiO_2$, and (d) 10 wt% $BiVO_4/TiO_2$.

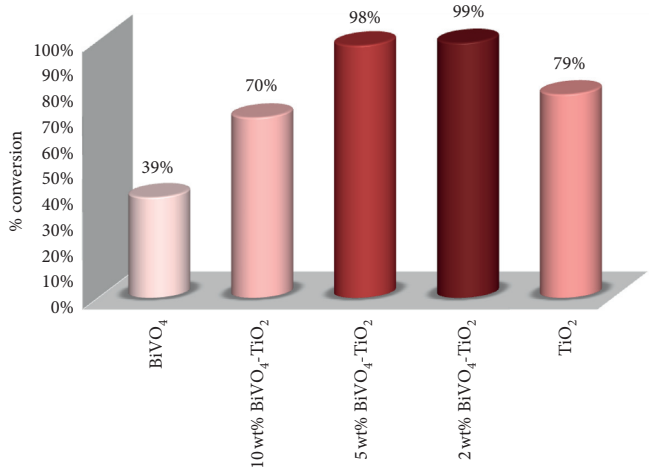

Figure 12: Photocatalytic conversion of methylene blue under solar light irradiation for the different catalysts.

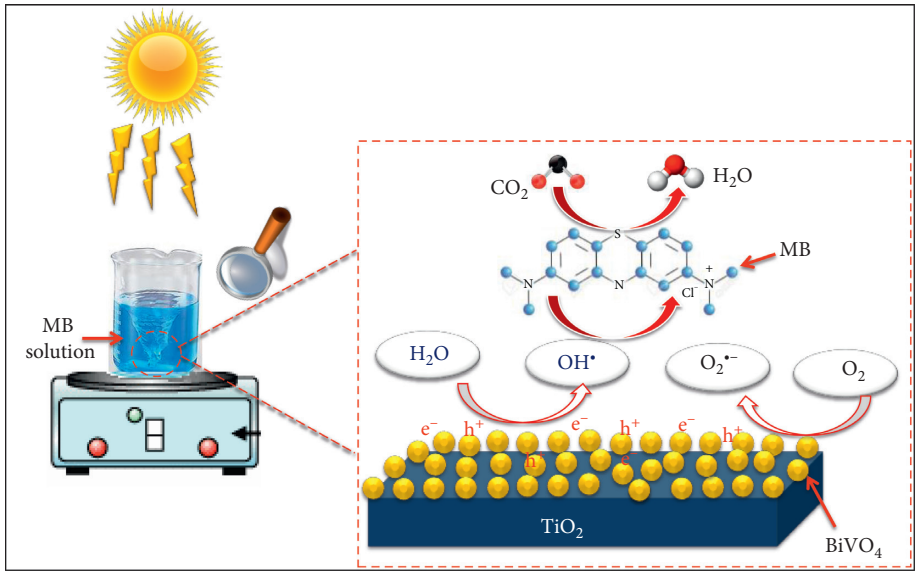

Scheme 1: Schematic illustration of methylene blue degradation.

scavenging the holes generated in the valence band, on the other hand. Moreover, Lv et al. [55] have reported that the surface lattice distortion on the titanium dioxide surface participates in the degradation of target pollutants by providing energy which is able to break the chemical bonds of organic molecules such as methylene blue.

4.1. Suggested Photocatalytic Mechanism. According to the previous results, the photocatalytic mechanism of $BiVO_4$/TiO_2 heterojunction can be explained as given in Scheme 1. The suggested mechanism of the photocatalytic oxidation of methylene blue is illustrated in Scheme 2.

After thermodynamic equilibrium, when the $BiVO_4$/TiO_2 composite is illuminated with photons having energy equal or greater than its band gap energy, electrons can promote from the valence band (VB) to the conduction band (CB) of $BiVO_4$ leaving a hole (h^+). By virtue of the joint of electric fields between two solids on the one hand and the CB edge potential of $BiVO_4$ which is more negative than that of TiO_2 on the other hand, the photoinduced electrons can be injected to the conduction band of TiO_2 (equation (2)) [55].

$$\frac{BiVO_4}{TiO_2} + h\nu \longrightarrow BiVO_4\left(h^+_{VB}\right) + TiO_2\left(e^-_{CB}\right). \quad (2)$$

Afterward, the injected electrons could capture the adsorbed O_2 and assisting its reduction into $O_2^{\bullet-}$ superoxide radicals. Thus, $O_2^{\bullet-}$ radicals react in turn with H_2O molecules and form hydroxyl ions (OH^-) and hydroperoxyl radicals ($HOO^{\bullet}$) (equations (3) and (4)) [56].

$$O_2 + e^-_{CB} \longrightarrow O_2^{\bullet-}, \quad (3)$$

$$O_2^{\bullet-} + H_2O_{ads} \longrightarrow HOO^{\bullet} + OH^-. \quad (4)$$

As well as, h^+ holes react with electron donors such as H_2O and OH^- anions adsorbed on the surface of the semiconductor and produce $OH^{\bullet}$ hydroxyl groups (equations (5) and (6)) [57].

$$H_2O_{ads} + h^+_{VB} \longrightarrow H^+ + OH^{\bullet}_{ads}, \quad (5)$$

$$OH^-_{ads} + h^+_{VB} = OH^{\bullet}_{ads}, \quad (6)$$

$$MB + OH^{\bullet}_{ads} \longrightarrow CO_2 + H_2O. \quad (7)$$

The formed radicals ($OH^{\bullet}$ and $O_2^{\bullet-}$) will participate in the degradation of adsorbed pollutants on the surface of the catalyst. Hence, it is obvious that $OH^{\bullet}$ radicals are the main oxidants in the photodecomposition of organic contaminants reactions. In fact, these species are endowed with high reactivity and strong oxidizing capability for the removal of organic targets into inorganic compounds such as CO_2, water, and organic chain acids (equation (7)) [58].

So far, it is well recognized that oxygen vacancies (V_O) promoted by the formed heterojunction act as a hole trapping center, resulting in the effective separation of photoinduced electron-hole pairs (equation (8)) [46]:

$$V_O^- + h^+ \longrightarrow V_O. \quad (8)$$

5. Reusability and Stability of $BiVO_4$/TiO_2 Nanocomposite

From a practical point of view, the stability and reusability study of the photocatalysts is of great importance in the field of wastewater purification. Therefore, the stability and reusability of the $BiVO_4$/TiO_2 nanocomposites could also be checked. In this concern, four cycles of photocatalytic MB degradation experiments via 2 wt% $BiVO_4$/TiO_2 composite were carried out under identical reaction conditions, and results are depicted in Figure 13. The 2 wt% $BiVO_4$/TiO_2 nanocomposite exhibited high efficiency and reusability; even the photocatalytic activities are 99.0%, 98.2%, 95.4%, and 89.7% after 1, 2, 3, and 4 successive

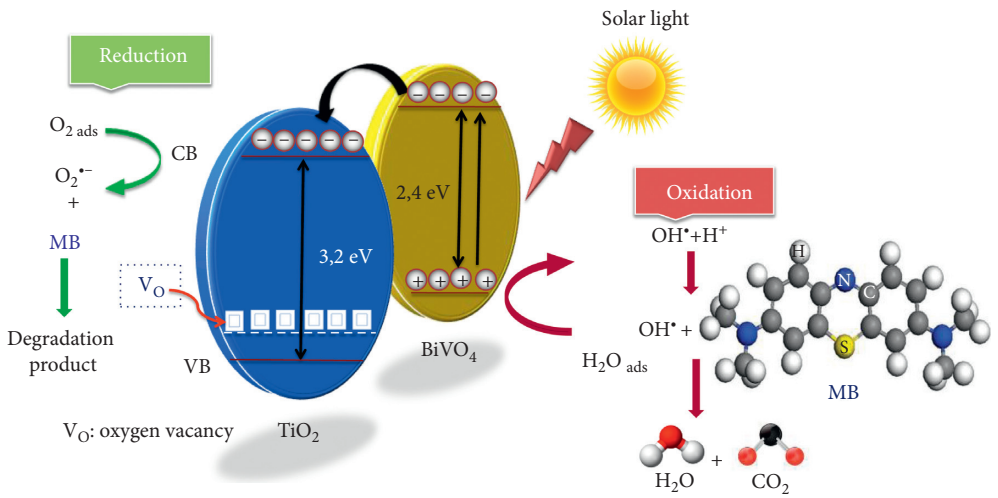

Scheme 2: Suggested photocatalytic mechanism of methylene blue degradation.

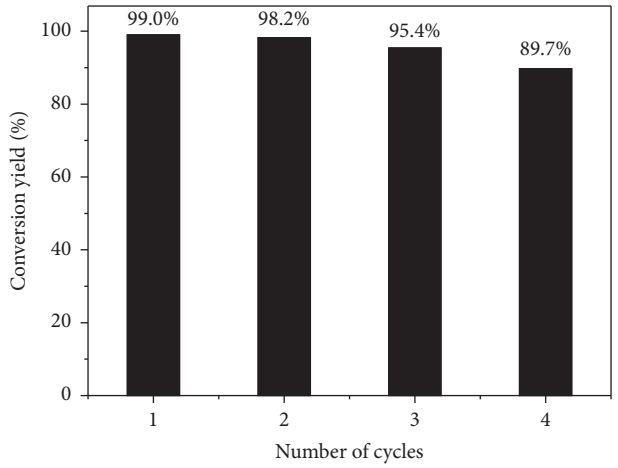

Figure 13: Reusability test of 2 wt% $BiVO_4/TiO_2$ photocatalyst.

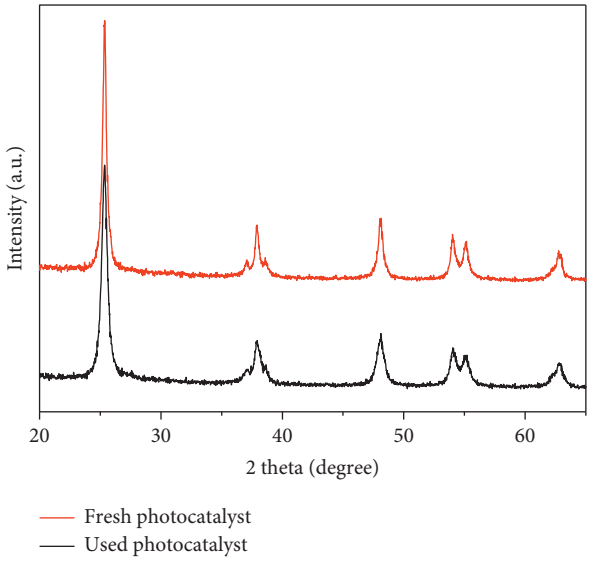

Figure 14: XRD patterns of fresh and used 2 wt% $BiVO_4/TiO_2$ photocatalyst.

cycles, respectively. The results show that the photocatalytic efficiency decreases but not significantly since the activity losses are 0.8%, 3.6%, and 9.4% (compared to the 1st cycle) indicating that the photocatalyst still maintains a high photodegradation capacity which reflects the high stability of the prepared nanocomposite. This result is advantageous to the recycling of $BiVO_4/TiO_2$ photocatalyst and decreasing the application cost.

The XRD patterns of fresh and used 2 wt% $BiVO_4/TiO_2$ photocatalyst (Figure 14) revealed that the four repeated uses do not affect the crystalline structure of anatase TiO_2 which is in good agreement with the high activity and stability of the catalyst.

6. Conclusion

In the present investigation, we systematically studied the effect of different $BiVO_4$ amounts on the structural, textural, and optical properties of $BiVO_4/TiO_2$ heterojunction materials which were elaborated by the one-pot hydrothermal method. The current outcomes elucidate that the creation of heterojunction between $BiVO_4$ and TiO_2 induces the

formation of more site defects on the catalyst surface. Furthermore, we have demonstrated that $BiVO_4$ could well control the crystallite size of solids. Indeed, controlling the size of the crystallites could be of great interest in our case by the fact that this latter makes possible to stabilize the anatase phase from easy transformation to rutile. Moreover, the optical behavior of as-prepared solids was drastically modified by shifting the absorption edge of TiO_2 to the visible light range. This effect might be explained by the fact that the presence of such defects enhances the charge carriers lifetime which leads to the amelioration of the catalytic efficiency. In order to achieve a better understanding of this system, the photoactivity of $BiVO_4/TiO_2$ materials was evaluated in the methylene blue degradation reaction. Results revealed that the amount of $BiVO_4$ in the $BiVO_4/TiO_2$ nanocomposite has a significant influence on the photoactivity of photocatalysts, and the highest degradation rate catalyst can be assigned to the 2 wt% $BiVO_4/TiO_2$ solid and it is equal to 99% after one hour of solar light irradiation. It is inferred to mention that such enhancement could be assigned to the controlled crystallite sizes, the interesting textural properties, and the attractive optical features of the catalysts. Furthermore, $BiVO_4/TiO_2$ photocatalyst displayed significant recyclability and stability for four catalytic cycles in the methylene blue photodegradation reaction. These results indicate that the nanocatalyst $BiVO_4/TiO_2$ can be used as a promising photocatalyst for the photocatalytic treatment of industrial wastewater.

Data Availability

The data used to support the findings of this study are available from the corresponding author upon request.

Conflicts of Interest

The authors declare that they have no conflicts of interest.

Authors' Contributions

Sahar Mansour was involved in conceptualization, validation, investigation, methodology, formal analysis, and writing—review and editing. Rym Akkari was involved in conceptualization, supervision, and writing—review and editing. Semy Ben Chaabene was involved in methodology, supervision, and writing—review and editing. Mongia Saïd Zina was involved in conceptualization, methodology, supervision, and writing—review and editing.

Acknowledgments

The authors gratefully acknowledge the financial support provided by the Tunisian Ministry of Higher Education and Scientific Research.

References

[1] A. D. Mauro, A. Landström, I. Concina, G. Impellizzeri, V. Privitera, and M. Epifani, "Surface modification by vanadium pentoxide turns oxide nanocrystals into powerful adsorbents of methylene blue," *Journal of Colloid and Interface Science*, vol. 533, pp. 369–374, 2019.

[2] D. Ghosh and K. G. Bhattacharyya, "Adsorption of methylene blue on kaolinite," *Applied Clay Science*, vol. 20, no. 6, pp. 295–300, 2002.

[3] J. H. Baek, B. J. Kim, G. S. Han et al., "$BiVO_4/WO_3/SnO_2$ double-heterojunction photoanode with enhanced charge separation and visible-transparency for bias-free solar water-splitting with a perovskite solar cell," *ACS Applied Materials & Interfaces*, vol. 9, no. 2, pp. 1479–1487, 2017.

[4] P. S. Kumar, M. Selvakumar, S. G. Babu, S. Induja, and S. Karuthapandian, "CuO/ZnO nanorods: an affordable efficient p-n heterojunction and morphology dependent photocatalytic activity against organic contaminants," *Journal of Alloys and Compounds*, vol. 701, pp. 562–573, 2017.

[5] A. Kusior, K. Michalec, P. Jelen, and M. Radecka, "Shaped $Fe2O_3$ nanoparticles—synthesis and enhanced photocatalytic degradation towards RhB," *Applied Surface Science*, vol. 476, pp. 342–352, 2019.

[6] X. Chang, Z. Li, X. Zhai et al., "Efficient synthesis of sunlight-driven ZnO-based heterogeneous photocatalysts," *Materials & Design*, vol. 98, pp. 324–332, 2016.

[7] D. Zheng, G. Zhang, and X. Wang, "Integrating CdS quantum dots on hollow graphitic carbon nitride nanospheres for hydrogen evolution photocatalysis," *Applied Catalysis B: Environmental*, vol. 179, pp. 479–488, 2015.

[8] J. Yu, Y. Yu, P. Zhou, W. Xiao, and B. Cheng, "Morphology-dependent photocatalytic H_2-production activity of CdS," *Applied Catalysis B: Environmental*, vol. 156-157, pp. 184–191, 2014.

[9] K. Chakraborty, S. Chakrabarty, P. Das, S. Ghosh, and T. Pal, "UV-assisted synthesis of reduced graphene oxide zinc sulfide composite with enhanced photocatalytic activity," *Materials Science and Engineering: B*, vol. 204, pp. 8–14, 2016.

[10] S. Mansour, S. Knani, R. Bensouilah, and Z. Ksibi, "Wastewater problems and treatments," in *Current Trends and Future Developments on (Bio-) Membranes*, A. Basile and K. Ghasemzadeh, Eds., Elsevier, pp. 151–174, Amesterdam, Netherland, 2020.

[11] R. Rahimi, E. Honarvar Fard, S. Saadati, and M. Rabbani, "Degradation of methylene blue via Co-TiO_2 nano powders modified by meso-tetra(carboxyphenyl)porphyrin," *Journal of Sol-Gel Science and Technology*, vol. 62, no. 3, pp. 351–357, 2012.

[12] S. Yousefzadeh, M. Faraji, and A. Z. Moshfegh, "Constructing $BiVO_4$/graphene/TiO_2 nanocomposite photoanode for photoelectrochemical conversion applications," *Journal of Electroanalytical Chemistry*, vol. 763, pp. 1–9, 2016.

[13] K. Wenderich and G. Mul, "Methods, mechanism, and applications of photodeposition in photocatalysis: a review," *Chemical Reviews*, vol. 116, no. 23, pp. 14587–14619, 2016.

[14] M. Meksi, H. Kochkar, G. Berhault, and C. Guillard, "Effect of cerium content and post-thermal treatment on doped anisotropic TiO_2 nanomaterials and kinetic study of the photodegradation of formic acid," *Journal of Molecular Catalysis A: Chemical*, vol. 409, pp. 162–170, 2015.

[15] W. Fang, M. Xing, and J. Zhang, "Modifications on reduced titanium dioxide photocatalysts: a review," *Journal of Photochemistry and Photobiology C: Photochemistry Reviews*, vol. 32, pp. 21–39, 2017.

[16] Y. Wang, J. Zhao, T. Wang et al., "CO_2 photoreduction with H_2O vapor on highly dispersed CeO_2/TiO_2 catalysts: surface species and their reactivity," *Journal of Catalysis*, vol. 337, pp. 293–302, 2016.

[17] Y. Bessekhouad, D. Robert, and J.-V. Weber, "Photocatalytic activity of Cu_2O/TiO_2, Bi_2O_3/TiO_2 and $ZnMn_2O_4/TiO_2$ heterojunctions," *Catalysis Today*, vol. 101, no. 3-4, pp. 315–321, 2005.

[18] Q. Xu, L. Zhang, J. Yu, S. Wageh, A. A. Al-Ghamdi, and M. Jaroniec, "Direct Z-scheme photocatalysts: principles, synthesis, and applications," *Materials Today*, vol. 21, no. 10, pp. 1042–1063, 2018.

[19] M. Zalfani, Z.-Y. Hu, W.-B. Yu et al., "$BiVO_4$/3DOM TiO_2 nanocomposites: effect of $BiVO_4$ as highly efficient visible light sensitizer for highly improved visible light photocatalytic activity in the degradation of dye pollutants," *Applied Catalysis B: Environmental*, vol. 205, pp. 121–132, 2017.

[20] T. R. A. Thara, P. P. Rao, S. Divya, A. K. V. Raj, and T. S. Sreena, "Enhanced near infrared reflectance with brilliant yellow hues in scheelite type solid solutions, $(LiLaZn)_{1/3}MoO_4$–$BiVO_4$ for energy saving products," *ACS Sustainable Chemistry & Engineering*, vol. 5, pp. 5118–5126, 2017.

[21] Y. Xue and X. Wang, "The effects of Ag doping on crystalline structure and photocatalytic properties of $BiVO_4$," *International Journal of Hydrogen Energy*, vol. 40, no. 17, pp. 5878–5888, 2015.

[22] X. Zhang, Z. Ai, F. Jia, L. Zhang, X. Fan, and Z. Zou, "Selective synthesis and visible-light photocatalytic activities of $BiVO_4$ with different crystalline phases," *Materials Chemistry and Physics*, vol. 103, no. 1, pp. 162–167, 2007.

[23] Y. Park, K. J. McDonald, and K.-S. Choi, "Progress in bismuth vanadate photoanodes for use in solar water oxidation," *Chemical Society Reviews*, vol. 42, no. 6, pp. 2321–2337, 2013.

[24] X. Song, Y. Li, Z. Wei, S. Ye, and D. D. Dionysiou, "Synthesis of $BiVO_4/P_{25}$ composites for the photocatalytic degradation of ethylene under visible light," *Chemical Engineering Journal*, vol. 314, pp. 443–452, 2017.

[25] O. Monfort, D. Raptis, L. Satrapinskyy, T. Roch, G. Plesch, and P. Lianos, "Production of hydrogen by water splitting in a photoelectrochemical cell using a $BiVO_4/TiO_2$ layered photoanode," *Electrochimica Acta*, vol. 251, pp. 244–249, 2017.

[26] X. Zhu, F. Zhang, M. Wang et al., "A shuriken-shaped m-$BiVO_4$/{0 0 1}–TiO_2 heterojunction: synthesis, structure and enhanced visible light photocatalytic activity," *Applied Catalysis A: General*, vol. 521, pp. 42–49, 2015.

[27] Y. Hu, D. Li, H. Wang, G. Zeng, X. Li, and Y. Shao, "Role of active oxygen species in the liquid-phase photocatalytic degradation of RhB using $BiVO_4/TiO_2$ heterostructure under visible light irradiation," *Journal of Molecular Catalysis A: Chemical*, vol. 408, pp. 172–178, 2015.

[28] R. Rangel, J. A. Cortés, J. Lara, P. Quintana, J. J. Alvarado-Gil, and O. Contreras, "Advantages of hydrothermal synthesis to produce tunable TiO_2 nanomicro sized photocatalysts and their effect in lignin degradation," *Nano*, vol. 10, no. 3, p. 1550046, 2015.

[29] Z. Jiao, H. Yu, X. Wang, and Y. Bi, "Ultrathin $BiVO_4$ nanobelts: controllable synthesis and improved photocatalytic oxidation of water," *RSC Advances*, vol. 6, p. 731360, 2016.

[30] Y. Zhang, Y. Guo, H. Duan, H. Li, C. Sun, and H. Liu, "Facile synthesis of V^{4+} self-doped, [010] oriented $BiVO_4$ nanorods with highly efficient visible light-induced photocatalytic activity," *Physical Chemistry Chemical Physics*, vol. 16, no. 44, pp. 24519–24526, 2014.

[31] K. Yang, X. Chen, Z. Zheng, J. Wan, M. Feng, and Y. Yu, "Solvent-induced surface disorder and doping-induced lattice distortion in anatase TiO_2 nanocrystals for enhanced photoreversible color switching," *Journal of Materials Chemistry A*, vol. 7, no. 8, pp. 3863–3873, 2019.

[32] H. Ullah, I. Khan, Z. H. Yamani, and A. Qurashi, "Sonochemical-driven ultrafast facile synthesis of SnO_2 nanoparticles: growth mechanism structural electrical and hydrogen gas sensing properties," *Ultrasonics Sonochemistry*, vol. 34, pp. 484–490, 2017.

[33] C. Regmi, Y. K. Kshetri, T.-H. Kim, R. P. Pandey, S. K. Ray, and S. W. Lee, "Fabrication of Ni-doped $BiVO_4$ semiconductors with enhanced visible-light photocatalytic performances for wastewater treatment," *Applied Surface Science*, vol. 413, pp. 253–265, 2017.

[34] I. Tbessi, M. Benito, J. Llorca, E. Molins, S. Sayadi, and W. Najjar, "Silver and manganese co-doped titanium oxide aerogel for effective diclofenac degradation under UV-A light irradiation," *Journal of Alloys and Compounds*, vol. 779, pp. 314–325, 2019.

[35] Y. Huo, J. Zhu, J. Li, G. Li, and H. Li, "An active La/TiO_2 photocatalyst prepared by ultrasonication-assisted sol-gel method followed by treatment under supercritical conditions," *Journal of Molecular Catalysis A: Chemical*, vol. 278, no. 1-2, pp. 237–243, 2007.

[36] X. Wang, Y. Shen, G. Zuo, F. Li, Y. Meng, and L. Hou, "Effect of pH and molar concentration on photocatalytic performance of $BiVO_4$ synthesised by sol-gel method," *Materials Research Innovations*, vol. 20, no. 7, pp. 500–503, 2016.

[37] W. Li, Z. Wang, D. Kong et al., "Visible-light-induced dendritic $BiVO_4/TiO_2$ composite photocatalysts for advanced oxidation process," *Journal of Alloys and Compounds*, vol. 688, pp. 703–711, 2016.

[38] M. Derbali, A. Othmani, S. Kouass, F. Touati, and H. Dhaouadi, "$BiVO_4/TiO_2$ nanocomposite: electrochemical sensor for hydrogen peroxide," *Materials Research Bulletin*, vol. 125, p. 110771, 2020.

[39] M. Thommes, K. Kaneko, A. V. Neimark et al., "Physisorption of gases, with special reference to the evaluation of surface area and pore size distribution (IUPAC technical report)," *Pure and Applied Chemistry*, vol. 87, no. 9-10, pp. 1051–1069, 2015.

[40] O. Bechambi, A. Touati, S. Sayadi, and W. Najjar, "Effect of cerium doping on the textural, structural and optical properties of zinc oxide: role of cerium and hydrogen peroxide to enhance the photocatalytic degradation of endocrine disrupting compounds," *Materials Science in Semiconductor Processing*, vol. 39, pp. 807–816, 2015.

[41] C. Gannoun, A. Turki, H. Kochkar et al., "Elaboration and characterization of sulfated and unsulfated V_2O_5/TiO_2 nanotubes catalysts for chlorobenzene total oxidation," *Applied Catalysis B: Environmental*, vol. 147, pp. 58–64, 2014.

[42] K. H. Reddy, S. Martha, and K. M. Parida, "Fabrication of novel p-BiOI/n-$ZnTiO_3$ heterojunction for degradation of rhodamine 6G under visible light irradiation," *Inorganic Chemistry*, vol. 52, no. 11, pp. 6390–6401, 2013.

[43] B. Baral, K. H. Reddy, and K. M. Parida, "Construction of M-$BiVO_4$/T-$BiVO_4$ isotype heterojunction for enhanced photocatalytic degradation of norfloxacine and oxygen evolution reaction," *Journal of Colloid and Interface Science*, vol. 554, pp. 278–295, 2019.

[44] Z. Guo, P. Li, H. Che et al., "One-dimensional spindle-like $BiVO_4/TiO_2$ nanofibers heterojunction nanocomposites with enhanced visible light photocatalytic activity," *Ceramics International*, vol. 42, no. 3, pp. 4517–4525, 2016.

[45] X. An, T. Li, B. Wen et al., "New insights into defect-mediated heterostructures for photoelectrochemical water splitting," *Advanced Energy Materials*, vol. 6, no. 8, p. 1502268, 2016.

[46] L. Mascaretti, V. Russo, G. Zoppellaro et al., "Excitation wavelength- and medium-dependent photoluminescence of reduced nanostructured TiO_2 films," *The Journal of Physical Chemistry C*, vol. 123, no. 17, pp. 11292–11303, 2019.

[47] M. Meksi, A. Turki, H. Kochkar, L. Bousselmi, C. Guillard, and G. Berhault, "The role of lanthanum in the enhancement of photocatalytic properties of TiO_2 nanomaterials obtained by calcination of hydrogenotitanate nanotubes," *Applied Catalysis B: Environmental*, vol. 181, pp. 651–660, 2016.

[48] J. Liu, J. Li, A. Sedhain, J. Lin, and H. Jiang, "Structure and photoluminescence study of TiO_2 nanoneedle texture along vertically aligned carbon nanofiber arrays," *The Journal of Physical Chemistry C*, vol. 112, no. 44, pp. 17127–17132, 2008.

[49] M. Hamandi, G. Berhault, F. Dappozze, C. Guillard, and H. Kochkar, "Titanium dioxide nanotubes/poly-hydroxyfullerene composites for formic acid photo-degradation," *Applied Surface Science*, vol. 412, pp. 306–318, 2017.

[50] R. P. Antony, T. Mathews, C. Ramesh et al., "Efficient photocatalytic hydrogen generation by Pt modified TiO_2 nanotubes fabricated by rapid breakdown anodization," *International Journal of Hydrogen Energy*, vol. 37, no. 10, pp. 8268–8276, 2012.

[51] N. Wetchakun, S. Chainet, S. Phanichphant, and K. Wetchakun, "Efficient photocatalytic degradation of methylene blue over $BiVO_4/TiO_2$ nanocomposites," *Ceramics International*, vol. 41, no. 4, pp. 5999–6004, 2015.

[52] A. P. Singh, N. Kodan, B. R. Mehta, A. Held, L. Mayrhofer, and M. Moseler, "Band edge engineering in $BiVO_4/TiO_2$ heterostructure: enhanced photoelectrochemical performance through improved charge transfer," *ACS Catalysis*, vol. 6, no. 8, pp. 5311–5318, 2016.

[53] A. K. L. Sajjad, S. Shamaila, B. Tian, F. Chen, and J. Zhang, "One step activation of WO_x/TiO_2 nanocomposites with enhanced photocatalytic activity," *Applied Catalysis B: Environmental*, vol. 91, no. 1-2, pp. 397–405, 2009.

[54] W. Wang, Y. Ye, J. Feng, M. Chi, J. Guo, and Y. Yin, "Enhanced photoreversible color switching of redox dyes catalyzed by barium-doped TiO_2 nanocrystals," *Angewandte Chemie International Edition*, vol. 54, no. 4, pp. 1321–1326, 2015.

[55] Y.-R. Lv, C.-J. Liu, R.-K. He, X. Li, and Y.-H. Xu, "$BiVO_4/TiO_2$ heterojunction with enhanced photocatalytic activities and photoelectochemistry performances under visible light illumination," *Materials Research Bulletin*, vol. 117, pp. 35–40, 2019.

[56] L. Shi, C. Xu, X. Sun et al., "Facile fabrication of hierarchical $BiVO_4/TiO_2$ heterostructures for enhanced photocatalytic activities under visible-light irradiation," *Journal of Materials Science*, vol. 53, no. 16, pp. 11329–11342, 2018.

[57] A. Touati, T. Hammedi, W. Najjar, Z. Ksibi, and S. Sayadi, "Photocatalytic degradation of textile wastewater in presence of hydrogen peroxide: effect of cerium doping Titania," *Journal of Industrial and Engineering Chemistry*, vol. 35, pp. 36–44, 2016.

[58] J. G. Pastora, S. Dominguez, E. Bringas, M. J. Rivero, I. Ortiz, and D. D. Dionysiou, "Review and perspectives on the use of magnetic nanophotocatalysts (MNPCs) in water treatment," *Chemical Engineering Journal*, vol. 310, pp. 407–427, 2016.